

AN ASME PUBLICATION  
\$4.00 per copy \$2.00 to ASME Members



80-WA/DSC-19

THE AMERICAN SOCIETY OF MECHANICAL ENGINEERS  
345 E 47 St., New York, N.Y. 10017

The Society shall not be responsible for statements or opinions advanced in papers or in discussion at meetings of the Society or of its Divisions or Sections, or printed in its publications. Discussion is printed only if the paper is published in an ASME Journal or Proceedings. Released for general publication upon presentation. Full credit should be given to ASME, the Technical Division, and the author(s).

# A Comparison of Natural Frequency Prediction Methods for Flexible Manipulator Arms

W. J. Book

M. Majette

School of Mechanical Engineering,  
Georgia Institute of Technology,  
Atlanta, Ga.

*Predictions of natural frequencies of flexible manipulator arms as performed by alternative structural models and computer implementations are compared. The Space Shuttle Remote Manipulator System (RMS) manipulator arm is used as the basis for comparison. Finite element and transfer matrix implementations of Bernoulli Euler, lumped mass, and consistent mass models are considered.*

## INTRODUCTION

One of the most interesting applications of manipulators to develop in recent years is the Remote Manipulator System (RMS) which has been designed for deployment on the Space Shuttle. This long (50 ft) lightweight (910 lbs.) arm shown schematically in Figure 1, will deploy and retrieve large payloads in space. The RMS is designed to deploy a maximum mass of 65 k lbs, although small payloads are more typical. The weightless conditions of space have enabled a combination of arm parameters not feasible in Earth's gravity. The RMS, for example, would not support its own weight in a one g environment.

The new ranges of parameters in mechanical arm design has required that the analysis of arm flexibility and resulting vibrations be performed with greater accuracy and confidence than required in previous arm designs. Realistic simulation of dynamic behavior must include consideration of the flexibility and nonlinear effects due to Coriolis and centrifugal forces. The resulting equations of motion are quite complex. Verification of models and simulations becomes correspondingly complex and must rely on separate verification of various aspects, flexibility for example. The comparison of natural frequencies and mode shapes provides an effective check on the accuracy of modeling any structure, including the RMS. Thus the various "complete" dynamic models can be compared in this one aspect to more conventional and precise models. This presumes the availability of a precise more or less conventional model which realistically represents the physical system, at least in some hypothetical configuration.

The object of this paper is to present a comparison of candidates for the "precise conventional model" for the RMS flexible, linear dynamics. Finite element models are compared to impedance models implemented with the transfer matrix approach. The hypothetical arm configuration has locked joints arranged to place the arm in a simple straight geometry. The end of the arm normally attached to the Shuttle Orbiter is specified as fixed. Payloads of 0 and 32 K lbs. are considered.

## FINITE ELEMENT ANALYSIS TECHNIQUES

In problems involving the modeling of a continuum the finite element approach has received effective and widespread application. A detailed introduction can be found in numerous books on the subject [1,2]. The structural dynamics problem is often dealt with using finite element techniques. The undamped structure is modeled by the matrix equation

$$\underline{M} \frac{d^2}{dt^2} \underline{x} + \underline{K} \underline{x} = 0$$

where  $\underline{M}$  is the structure's mass matrix,  $\underline{K}$  is the structure's stiffness matrix, and  $\underline{x}$  is a displacement vector of the structure from the equilibrium position. The eigenproblem can be formulated as

$$\underline{M}^{-1} \underline{K} \hat{\underline{x}} = \omega^2 \hat{\underline{x}} \quad (1)$$

where  $\omega^2$  is an eigenvalue, the square of a structure natural frequency and  $\hat{\underline{x}}$  is the corresponding eigenvector, corresponding to the mode shape.

Standard matrix techniques can be used to find  $\omega^2$  and  $\hat{\underline{x}}$ . The finite element techniques are used to find  $\underline{M}$  and  $\underline{K}$  from the structure geometry and material properties. A number of computer programs including NASTRAN [3] and STARDYNE are available to implement the users specification of the structure in a form suitable for defining and solving equation

Contributed by the Dynamic Systems & Control Division of The American Society of Mechanical Engineers for presentation at the Winter Annual Meeting, November 16-21, 1980, Chicago, Illinois. Manuscript received at ASME Headquarters July 19, 1980.

(1). The user's choice in this process includes the selection of the number and type of elements which determines the dimension and accuracy of the problem.

The compliance (stiffness) of the RMS is modeled by "bar" elements for the long slender beam like components, and point rotational compliances for the more concentrated compliance effects at the joint structures. (For the K matrix of the planar bar element see Appendix I).

The mass effects in the RMS are modeled by lumped mass elements and by consistent mass elements. The lumped mass element assumes all inertial effects are concentrated at a point. The consistent mass element is obtained by assuming mass is distributed along a beam element and moves in the manner consistent with the deflection assumed in obtaining the stiffness matrix of the bar element. Under certain conditions, a simple cantilever beam for instance, the consistent mass matrix gives a very good estimate of natural frequency with a small number of elements. For the planar case of the consistent mass element, the matrix  $\underline{M}$  is given in the Appendix I.

#### IMPEDANCE ANALYSIS VIA TRANSFER MATRIX TECHNIQUES

An alternative approach to linear problems in a one dimensional continuum is the transfer matrix implementation of impedance methods. A detailed description of these methods may be found in [4]. The vector  $\underline{Z}_0$  of significant physical variables (state variables) at one point in the continuum (point 0) are related to the variables  $\underline{Z}_1$  at another point (point 1) by a transfer matrix  $\underline{I}_1(\omega)$

$$\underline{Z}_0 = \underline{I}_1(\omega) \underline{Z}_1,$$

where the dependence of  $\underline{I}_1$  on the frequency variable  $\omega$  is shown. The transfer matrix  $\underline{I}_1$  is developed from the Laplace or Fourier transform of the linear differential equations, which may be ordinary or partial. The points 0 and 1 are the boundaries of the continuum, and the variables  $\underline{Z}_0$  and  $\underline{Z}_1$  are the boundary values. Two elements may share one boundary and the resulting system can be described with a transfer matrix which is the product of the transfer matrices of the separate elements, i.e. if additionally

$$\underline{Z}_1 = \underline{I}_2(\omega) \underline{Z}_2$$

then

$$\underline{Z}_0 = \underline{I}_1(\omega) \underline{I}_2(\omega) \underline{Z}_2$$

This process of eliminating state variables at intermediate boundaries can continue until a boundary is reached at which one half of the variables are prespecified to the zero. In this case  $n/2$  homogeneous equations, linear in the remaining  $n/2$  variables on the right hand side, can be found among the original  $n$  equations

$$\underline{Z}_0 = \underline{I}(\omega) \underline{Z}_N$$

and written as

$$\underline{0} = \tilde{\underline{I}}(\omega) \tilde{\underline{Z}}_N \quad (2)$$

where  $\tilde{\underline{I}}$  is an  $n/2 \times n/2$  submatrix of  $\underline{I}$  and  $\tilde{\underline{Z}}_N$  contains the  $n/2$  unspecified variables in  $\underline{Z}_N$ . A nontrivial solution of (2) requires that the frequency determinant  $\det[\tilde{\underline{I}}(\omega)] = 0$ . Those values of

$\omega = \omega_n$  in a structural system which satisfy  $\det[\tilde{\underline{I}}(\omega)] = 0$  are the natural frequencies of the system. Since  $\det[\tilde{\underline{I}}(\omega)]$  generally involves complex transcendental relationships, the natural procedures are used to find its roots, the natural frequencies. The values of  $\underline{Z}$  which result throughout the system when the frequency determinant is zero can be determined to an arbitrary factor and constitute the structure's modal shapes.

The advantage of the transfer matrix approach is that the analytical solution of partial differential equations which describe structural behavior can be used. For example a Bernoulli-Euler or Timoshenko beam model, which has known solutions in terms of arbitrary boundary conditions can be represented exactly in transfer matrix form. The numerical evaluation of the frequency determinant and the solution of  $\omega_n$  introduces accuracy limitations, of course.

The transfer matrix approach cannot be easily generalized to continua in two or more dimensions as can be the finite element approach, and the transform techniques employed apply only to linear dynamic behavior. These restrictions are not limiting here. Computer code for solving for  $\omega_n$  and the mode shapes as well as performing other available transfer matrix analysis is not generally available, but has been developed in the ongoing research. The resulting package, DSAP (Distributed Systems Analysis Package) is described in [5].

Other elements can be modeled with DSAP including the lumped mass, massless beam stiffness and point rotary stiffness, all of which are described in [4]. In addition the transfer matrix equivalent to the combination "bar" element and consistent mass matrix is developed in the Appendix I.

The dimension  $n$  of  $\underline{Z}$  needed to represent system behavior is important as it influences the cost of computer analysis. For a planar Bernoulli Euler beam model  $n = 4$ . For a spatial beam model including bending in two planes, torsion, and compression,  $n = 12$ .

#### COMPARISON STRATEGY

A study was undertaken to compare the natural frequency predictions by the DSAP transfer matrix approach and the finite element predictions using alternative elements to model the physical system. The ultimate purpose of the study was verification of dynamic models of the RMS manipulator arm. Specifically, the questions to be answered included:

1. What differences in natural frequencies are to be expected inherently due to the beam model, i.e., Bernoulli-Euler, bar and lumped mass, or bar and consistent mass?
2. What differences in predicted natural frequency are inherently due to the model implementation, i.e. finite element or transfer matrix?
3. How does natural frequency predicted vary with number of lumped masses used to represent a beam?
4. How do the mode shapes predicted by finite element and transfer matrix approaches compare?

The analysis using DSAP performed by the authors was compared to the finite element analysis performed by Allan Abelow at Charles Stark Draper Laboratory, Inc. (CSDL) and reported in [6].

TABLE 1. Beam Models, Implementations and Applications Considered.

Implementation	Application	B E A M M O D E L					
		Consistent Mass		Lumped Mass		Bernoulli-Euler	
		Planar	Spatial	Planar	Spatial	Planar	Spatial
Finite Element	RMS	X	ASAD/ CSDL Table 4	X	NASTRAN/ CSDL Table 6	X	X
	Cantilever	Table 2	X	Table 2	X	X	X
DSAP	RMS	Table 3	X	X	Table 5a & b	Table 5c Table 3	Table 5a & b Table 5c Table 6
	Cantilever	Table 2	X	Table 2	X	Table 2 (exact)	X

X - No analysis performed

In order to answer these questions a simple comparison for a cantilever beam vibrating in one plane was first made. This enabled an unambiguous choice of element parameter values not possible with the more complicated RMS structure. It also allowed comparison to exact analytical values corresponding to a Bernoulli-Euler beam model. These exact values were identical with the values found by DSAP with a Bernoulli-Euler model.

For RMS models, decisions were necessary on the details of implementing the model. For example, how does one represent joint stiffnesses, with point rotational springs or short beam segments? In general the DSAP models were chosen to correspond with the CSDL report. An exception is with the DSAP consistent mass implementation. For simplicity only a planar version of this element was implemented in DSAP. Thus exact comparison with CSDL's spatial results is not possible. In addition a new model called the DSAP RMS model was constructed not to imitate the finite element models but to capitalize on the strengths of the transfer matrix approach.

The beam models, computer implementations of the models, and configurations analyzed are summarized in Table 1.

COMPARISON OF CONSISTENT MASS, LUMPED MASS AND BERNOULLI-EULER MODELS AND IMPLEMENTATIONS

Comparisons of consistent mass and lumped mass beam models were performed for a simple cantilever case, varying the number of lumps, for DSAP and finite element implementations. Planar models of the RMS were compared for both models with only the

DSAP implementation. For the S configuration these natural frequencies correspond roughly to certain spatial modes as discussed elsewhere.

Table 2 shows the comparisons of the first natural frequency for the simple cantilever beam. Note that the two implementations of the lumped mass model converge to the respective exact values at the same rate as the number of elements is increased. (The exact values differ slightly due to slightly different parameter values.) The two implementations of the consistent mass model also converge similarly. The Bernoulli-Euler model yields the exact analytical solution to this problem.

Table 3 shows how the beam models affect the planar RMS models. In particular the Bernoulli-Euler and consistent mass models are compared for the first five modes. The 0 K and 32 K payloads are considered. The consistent mass model agrees best at the lowest natural frequencies. This is explained by the number of lumps between two nodes. The models agree better for larger payloads where the beam mass is less significant. Table 4 shows ASAD/CSDL frequencies for a spatial RMS model with the 32 K payload. As the planar model does not have some flexural or torsional modes some frequencies are not predicted by the planar model.

COMPARISON OF LUMPED VS. DISTRIBUTED PARAMETER (BERNOULLI-EULER) BEAM MODELS (DSAP IMPLEMENTATION)

In this comparison the effect of differences arising from the use of lumped versus distributed parameter beam elements on natural frequencies as computed by DSAP was studied. A series of models

TABLE 2. Simple Cantilever Beam Frequencies (rad/sec)

No. of Elements	DSAP		Draper Finite Elements	
	Lumped Mass	Consistent Mass	Lumped Mass	Consistent Mass
1	13.90	20.0361	13.900	20.048
3	18.99	19.9433	18.986	19.955
5	19.59	19.9416	19.593	19.953
10	19.86	19.9413	19.862	19.953
Exact	19.9413		19.9516	
Density/length	$\frac{1}{386 \times 12} \text{ lb}_f \text{ sec}^2 / \text{in}^2$		$\frac{1}{32.2 \times 144} \text{ lb}_f \text{ sec}^2 / \text{in}^2$	
EI	144 $\text{lb}_f \text{ in}^2$			
Length	12 in.			

TABLE 3. Comparison of Planar Distributed Mass (BTM4) and Consistent Mass (CMTM4) Models Via NFREQ.

Model: Shuttle manipulator arm - ASAD formulation Planar model of the arm in the  $X_0^R - Z_0^R$  plane (see Fig. 9, p. 23, of R-1210).

Case 1: No Payload

Mode	$\omega_{\text{BTM4}} \left( \frac{\text{rad}}{\text{sec}} \right)$	$\omega_{\text{CMTM4}} \left( \frac{\text{rad}}{\text{sec}} \right)$	% diff.
1	3.4491009	3.4491856	.0025
2	26.188285	26.276381	.3364
3	80.274321	83.939387	4.5657
4	144.44117	151.54090	4.9153
5	221.52522	252.00381	13.758
6	340.56842	393.77365	15.622
7	465.79030	641.59481	37.743

Case 2: With 32 K Payload

Mode	$\omega_{\text{BTM4}} \left( \frac{\text{rad}}{\text{sec}} \right)$	$\omega_{\text{CMTM4}} \left( \frac{\text{rad}}{\text{sec}} \right)$	% diff.
1	0.25153930	0.25153930	0
2	2.2758455	2.2758469	$6 \times 10^{-5}$
3	24.607993	24.703634	0.389
4	78.725394	82.439882	4.72
5	145.22091	152.44357	4.97

TABLE 4. ASAD/CSDL Frequencies (Table IV, p. 8, R-1210; Config. S)

Mode #	$\omega$ (Hz)	$\omega$ (Rad/sec)
1	.0337	.2117
2	.0424	.2664
3	.0594	.3732
4	.1206	.7578
5	.3677	2.3103
6	3.5164	22.0942
7	4.1033	25.7818
8	12.2208	76.7856
9	13.4454	84.4799
10	13.8032	86.7281

based on the CSDL/NASTRAN finite element representation were examined.

The initial case consisted only of the two long beams, ARM1 and ARM2 and their connections described by cbars 8-17 and the masses at nodes 9-18, (See Appendix II). In each successive case, additional elements were added so that the last case included the complete RMS with the exception of joint angles (e.g. no swingout or offset) and payload.

For each case, two sets of natural frequencies were computed. "Exact" frequencies were found by representing ARM1 (cbars 8-11, masses 9-12) and ARM2 (cbars 14-17, masses 15-18) as distributed parameter beams (Bernoulli-Euler/spatial). Next, "lumped" frequencies were found by representing ARM1 and ARM2 with lumped elements. In both instances lumped elements were used for all remaining model elements. Also, for the "lumped" frequencies, additional runs having ten and eighteen lumped parameter beams in ARM1 and ARM2 were made to demonstrate convergence to the "exact" frequencies.

Element parameters were taken from Table VI, VII, and VIII of report R-1210 [6] and are repeated in Appendix II. The only additional parameter needed was a mass per unit length for the distributed parameter beams, which was computed as shown below.

$$\text{Mass/unit length} = \sum \text{lumped mass/total length}$$

$$\begin{aligned} \text{For ARM1} &= \frac{4 \left( .0603 \frac{\text{lb}_f \text{ sec}^2}{\text{in}} \right)}{197.084 \text{ in}} \\ &= 1.2238 \times 10^{-3} \frac{\text{lb}_f \text{ sec}^2}{\text{in}^2} \end{aligned}$$

In lumped models having more than four divisions in ARM1 or ARM2, the individual massless beam lengths and concentrated masses were found as follows:

$$\text{Element length} = \text{total length}/\# \text{ elements}$$

$$\text{Element mass} = \text{total mass}/\# \text{ elements.}$$

For each case only the first two natural frequencies were found. The "lumped" frequencies were compared to the "exact" frequencies on a percentage error basis as follows:

$$\% \text{ error} = \frac{\omega \text{ "exact"} - \omega \text{ "lumped"}}{\omega \text{ "exact"}} \times 100$$

The results for these comparisons are shown in Table 5a. Additionally, some higher frequencies were computed for the final model (cbar 1 - node 25). These are listed in Table 5b.

As can be seen, agreement between the distributed and lumped models was good. The division of ARM1 and ARM2 into finer elements resulted in a better approximation of the "exact" frequencies. However, as more elements were added, the number of lumps needed in ARM1 and ARM2 for a good approximation decreased, so that in the last case (cbar 1 - node 25) four lumps per arm gave good answers. Notice that "lumped" frequencies generally were lower than "exact" ones. This was not true always though, as can be seen in modes 7 and 8 of Table 5b. Table 5b also illustrates that a given lumped model's accuracy decreases gradually for higher modes.

A final check on the accuracy of the spatial elements discussed above was performed using DSAP's planar element subroutines. The final case (cbar 1 - node 25) was used, with ARM1 and ARM2 represented by planar Bernoulli-Euler distributed beams. Again, the remaining model elements were lumped parameter elements. The resulting frequencies, listed in Table 5c, are in agreement with the "exact" spatial frequencies in Tables 5a and 5b.

DSAP Analysis of the RMS/S Configuration, 32K Payload

A DSAP analysis of the RMS in the S-configuration with 32-K payload is presented in this section. The modified representation of the arm used with DSAP is first outlined. Resulting natural frequencies and mode shapes are discussed and compared to those from the CSDL/Nastran finite element analysis. Conclusions and areas of further investigation follow.

DSAP RMS Model. The RMS model used with DSAP is taken from the CSDL/Nastran finite element model specified in figure 3 and tables VI, VII, and VIII in CSDL report R-1210. [7]. (See Appendix II). The only modification is that ARM1 and ARM2 are represented as distributed parameter Bernoulli Euler beams. These are assumed to consist of, respectively, cbars 8-11 and masses 9-12, and cbars 14-17, and masses 15-18. Thus the only additional parameter needed, mass per unit length, results as follows:

TABLE 5a. "Exact" vs. "Lumped" Natural Frequencies; Modes 1 & 2

# Lumps ARM1, ARM2	$\omega_1$ (rad/sec)	$\omega_2$ (rad/sec)	% error	
			$\omega_1$	$\omega_2$
cbar 8 - node 18				
exact	17.05	17.44	----	----
4	15.73	16.17	7.7	7.3
10	16.49	16.89	3.3	3.2
18	16.70	17.10	2.1	1.9
cbar 7 - node 19				
exact	8.115	8.452	----	----
4	7.893	8.225	2.74	2.69
10	8.023	8.358	1.13	1.11
18	8.058	8.393	0.91	0.94
cbar 5 - node 21				
exact	4.080	4.236	----	----
4	4.037	4.191	1.05	1.06
10	4.062	4.217	0.44	0.45
18	4.068	4.224	0.29	0.28
cbar 3 - node 23				
exact	2.168	2.484	----	----
4	2.151	2.464	0.78	0.80
10	2.161	2.476	0.32	0.32
18	2.164	2.479	0.18	0.20
cbar 1 - node 25				
exact	1.839	2.120	----	----
4	1.828	2.107	0.60	0.61
10	1.834	2.115	0.27	0.24
--	-----	-----	----	----

TABLE 5b. "Exact" vs. "Lumped" Natural Frequencies; Modes 3-10

Mode #	$\omega_{\text{exact}}$ (rad/sec)	$\omega_{\text{lump4}}$	$\omega_{\text{lump10}}$	% error	
				lump4	lump10
3	19.39	19.29	19.34	0.52	0.26
4	20.55	20.47	20.50	0.34	0.24
5	50.48	49.96	50.25	1.03	0.46
6	52.46	51.96	52.20	0.95	0.49
7	118.3	121.4	119.1	2.62	0.68
8	122.9	126.0	123.7	2.52	0.65
9	189.0	185.1	186.0	2.06	1.59
10	197.3	192.9	193.9	2.23	1.72

TABLE 5c. "Exact" Planar Natural Frequencies

$\omega(\text{PLANE1})$ (rad/sec)	$\omega(\text{PLANE2})$ (rad/sec)
2.12	1.839
19.39	20.55
50.48	52.46
122.90	118.30
189.00	197.30

$$H_{\text{ARM1}} = \frac{\sum_{i=9}^{12} M_i}{\text{total length}} = \frac{4(.0603) \frac{1b_f \text{ sec}^2}{\text{in}}}{197.084 \text{ in}}$$

$$H_{\text{ARM1}} = .0012238 \frac{1b_f \text{ sec}^2}{\text{in}^2}$$

$$H_{\text{ARM2}} = \frac{\sum_{i=15}^{18} M_i}{\text{total length}} = \frac{4(.0435) \frac{1b_f \text{ sec}^2}{\text{in}}}{225.984 \text{ in}}$$

$$H_{\text{ARM2}} = .00077 \frac{1b_f \text{ sec}^2}{\text{in}^2}$$

All remaining elements are unchanged; e.g., they remain lumped parameter elements. Offset and swingout are included, and the orbiter is assumed to be fixed.

Natural Frequencies. The first ten natural frequencies resulting from the DSAP analysis are listed in Table 6. CSDL/NASTRAN finite element natural frequencies, from Table III or report R-1210 [7] also appear in Table 6. The two sets of frequencies are compared on a percentage error basis as follows:

$$\% \text{ error} = \frac{|\omega_{\text{DSAP}} - \omega_{\text{CSDL}}|}{\omega_{\text{CSDL}}} \times 100$$

Agreement is good for modes one through eight. Modes nine and ten differ significantly, however. The difference is greater than would be expected between lumped and distributed parameter ARM1 and ARM2 formations on the basis of previous comparisons. A comparison of predicted shapes shows very little difference in the two models, even for modes nine and ten.

SUMMARY

Close agreement has been found in general between the DSAP and CSDL/NASTRAN implementations of the RMS in the S configuration with a 32K payload. The exception to this statement being the ninth and tenth modes which differed significantly. Further comparison of the DSAP/RMS model with a DSAP implemented lumped parameter model indicates that the lumped approximation to the long beams is not the source of the difference. The implementation (DSAP vs. NASTRAN) remains the prime explanation.

The influence of consistent mass elements, lumped mass elements, and of lumps has been demonstrated for both the cantilever beam and RMS models.

TABLE 6. DSAP vs. CSDL Natural Frequencies S Configuration, 32K Payload

Mode #	$\omega_{\text{DSAP}}$ (rad/sec)	$\omega_{\text{DSAP}}$ (Hz)	$\omega_{\text{CSDL}}$ (Hz)	% error
1	0.16596	0.02641	0.0264	0.04
2	0.19981	0.03180	.0317	0.32
3	0.31206	0.04967	0.0496	0.14
4	0.62756	0.09988	0.0989	0.99
5	1.90285	0.30285	0.3056	0.90
6	19.04636	3.03132	2.9949	1.22
7	19.90507	3.16799	3.1509	0.54
8	23.57887	3.75269	3.7399	0.34
9	54.51850	8.67689	11.3379	23.47
10	55.08199	8.76657	11.5510	24.10

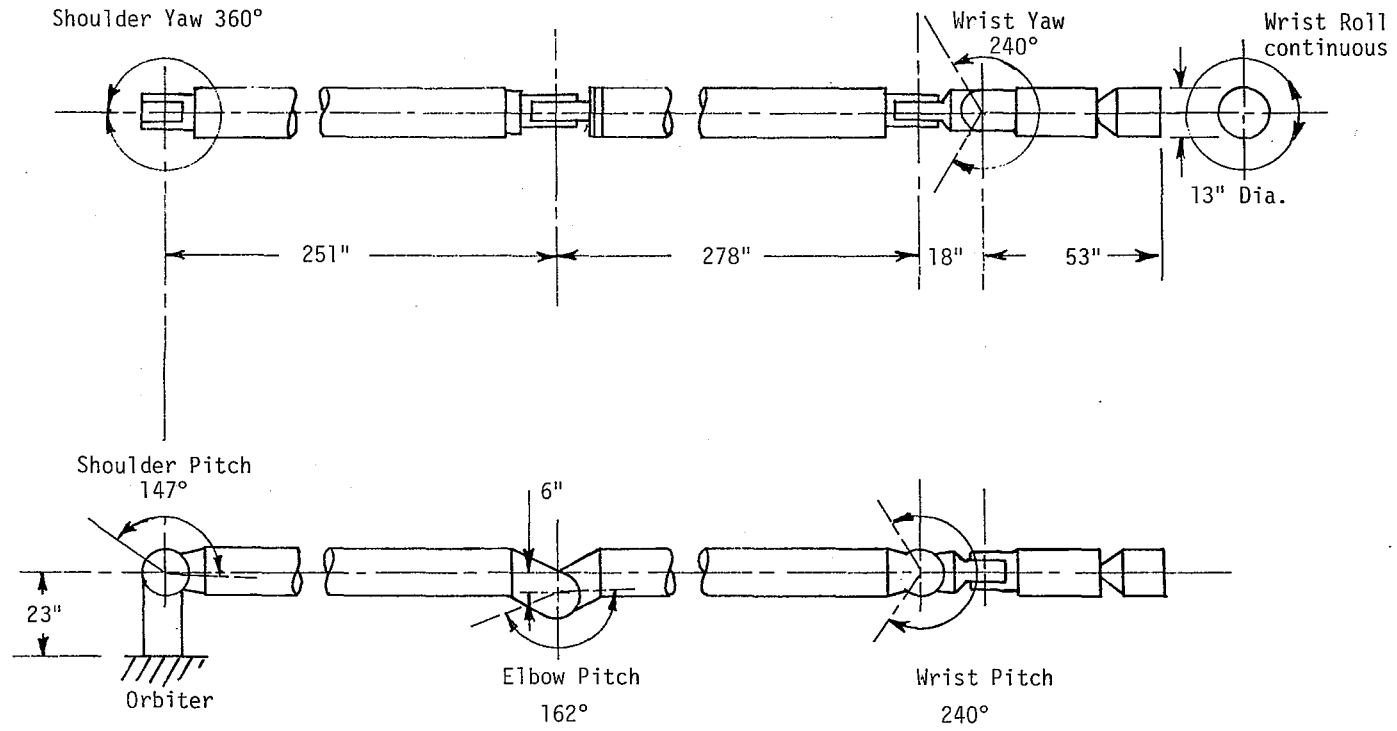


Fig. 1. Schematic of RMS with Approximate Dimensions. (To Approximate Scale)

REFERENCES

1. Cook, Robert D., Concepts and Applications of Finite Element Analysis, John Wiley and Sons, Inc., New York, 1974.
2. Desai, C. and J. Abel, Introduction to the Finite Element Method, Van Nostrand - Reinhold, New York, 1972.
3. McCormick, C. W. (Editor), NASTRAN User's Manual, MacNeal Schwindler Corp., May 1976.
4. Pestel, Edward C. and Frederick Leckie, Matrix Methods in Elastomechanics, McGraw Hill Book Co., Inc., New York, 1963.
5. Book, Wayne J., Mark Majette, and Kong Ma, "Distributed Systems Analysis Package (DSAP) and Its Application to Modeling Flexible Manipulators", Georgia Institute of Technology School of Mechanical Engineering, Final Report Project E25-603 Contract to Charles Stark Draper Laboratory, July, 1979.
6. Abelow, Allan V., "Comparisons of Remote Manipulator System Finite Element Models", Charles Stark Draper Laboratory, Inc., Cambridge, MA 02139, Report R-1210, November 1978.

APPENDIX I

Planar Beam Transfer Matrix with Consistent Mass Beam Model

The consistent mass matrix and the "BAR" element stiffness matrix used in finite element analysis were combined to obtain a dynamic stiffness matrix. The stiffness matrix can be converted directly to a transfer matrix for the element.

The consistent mass matrix for a beam as given on P. 256 of Concepts and Applications of Finite Element Analysis by Robert Cook, John Wiley & Sons, 1974 [1] is

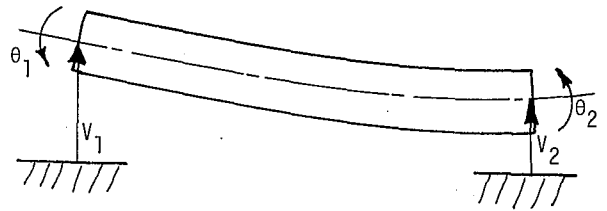
$$[m] = \frac{\rho A}{420} \begin{Bmatrix} 156L & 22L^2 & 54L & -13L^2 \\ 22L^2 & 4L^3 & 13L^2 & -3L^3 \\ 54L & 13L^2 & 156L & -22L^2 \\ -13L^2 & -3L^3 & -22L^2 & 4L^3 \end{Bmatrix}$$

where  $\rho$  = mass density per unit volume  
 $A$  = cross sectional area  
 $L$  = beam length

The displacement vector for the element is:

$$d = \begin{Bmatrix} v_1 \\ \theta_1 \\ v_2 \\ \theta_2 \end{Bmatrix} = \begin{Bmatrix} \text{translation, end 1} \\ \text{rotation, end 1} \\ \text{translation, end 2} \\ \text{rotation, end 2} \end{Bmatrix} = \begin{Bmatrix} d_{i-1} \\ d_i \end{Bmatrix}$$

where the sign conventions are given in the following figure.



The stiffness matrix for the planar BAR element is

$$[k] = \frac{EI}{L^3} \begin{Bmatrix} 12 & 6L & -12 & 6L \\ 6L & 4L^2 & -6L & 2L^2 \\ -12 & -6L & 12 & -6L \\ 6L & 2L^2 & -6L & 4L^2 \end{Bmatrix}$$

where  $E$  = Young's modulus for the material

$I$  = Cross section area moment of inertia

The dynamic stiffness matrix  $K_d$  relates the displacement vector to the force vector  $p$  on the element assuming harmonic motion with frequency  $\omega$  (or equivalent for this case, Fourier transform the differential equations).

$$[m] \ddot{d} + [k] d = p$$

$$\{ [k] - \omega^2 [m] \} d = p$$

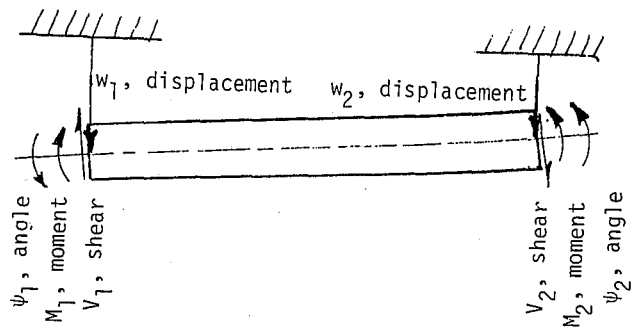
$$K_d(\omega) = \{ [k] - \omega^2 [m] \}$$

where

$$p = \begin{Bmatrix} \text{Shear force on end 1} \\ \text{Moment on end 1} \\ \text{Shear force on end 2} \\ \text{Moment on end 2} \end{Bmatrix} = \begin{Bmatrix} p_{i-1} \\ p_{i-2} \end{Bmatrix}$$

The sign conventions on  $p$  are in the same directions indicated for  $d$ .

The sign conventions for displacements and forces for the transfer matrix representation differ and are given as



Incorporating these differences we find

$$K_d = \begin{Bmatrix} -(12C-156BL) & 6LC-22L^2B & -(-12C-54LB) & 6LC+13L^2B \\ 6LC-22L^2B & -(4L^2C-4L^3B) & -6LC-13L^2B & -(2L^2C+3L^3B) \\ -12C-54LB & -(6LC-13L^2B) & 12C-156LB & -(-6LC+22L^2B) \\ -(6LC+13L^2B) & 2L^2C+3L^3B & -(-6LC+22L^2B) & 4L^2C-4L^3B \end{Bmatrix}$$

$$\text{where } B = \frac{\rho A \omega^2}{420}, \quad C = \frac{EI}{L^3}$$

The terms in parenthesis exhibit a net sign change in the change of sign conventions.

To obtain the transfer matrix denote

$$\begin{bmatrix} p_{i-1} \\ p_i \end{bmatrix} \begin{bmatrix} Q & R \\ -R^T & S \end{bmatrix} \begin{bmatrix} d_{i-1} \\ d_i \end{bmatrix} = K_d \begin{bmatrix} d_{i-1} \\ d_i \end{bmatrix}$$

Where  $p$  and  $d$  denote generalized force and displacement vectors in transfer matrix coordinates, i.e.

$$\underline{p} = \begin{bmatrix} W \\ \psi \end{bmatrix}, \quad \underline{d} = \begin{bmatrix} V \\ M \end{bmatrix}$$

By collecting variables at the same point on the same side of the equation, one obtains

$$\begin{bmatrix} \underline{d} \\ \underline{p} \end{bmatrix}_i = \begin{bmatrix} -R^{-1} & Q \\ -R^{-1} & -SR^{-1}Q \end{bmatrix} \begin{bmatrix} R^{-1} \\ SR^{-1} \end{bmatrix} \begin{bmatrix} \underline{d} \\ \underline{p} \end{bmatrix}_{i-1}$$

The standard for the transfer matrix state vector for a planar beam element is

$$z = \begin{Bmatrix} -W \\ \psi \\ M \\ V \end{Bmatrix}$$

which requires reversing the order of  $M$  and  $V$  and negating  $w$ .

## APPENDIX II

### Details of RMS Models

Two finite elements models described in [6] were used for comparison to the transfer matrix model implementations. They are termed in this paper the NASTRAN/CSDL and ASAD/CSDL although both were implemented in NASTRAN. NASTRAN/CSDL is a pure finite element model implemented by Abelow to most closely approximate the RMS physical system. ASAD/CSDL is implemented to most nearly approximate a full nonlinear, flexible dynamic (All Singing All Dancing or ASAD) model implemented by SPAR Aerospace Products Ltd. which has designed the RMS.

### NASTRAN/CSDL Model Details.

1. Sixteen beam elements,  $CBAR_i$  ( $i=1, \dots, 24$  and  $i \neq 8, 9, 10, 11, 14, 15, 16, 17$ ) representing joint flexibility.
2. The upper and lower arm beams ( $ARM1$  and  $ARM2$ ),  $CBAR_i$  ( $i=8, \dots, 11, 14, \dots, 17$ ) discretized into four elements each, representing their flexibility.
3. Rigid beam element representing the payload  $RBAR_1$ .
4. Rigid beam element representing the orbiter,  $RBAR_2$ .

The NASTRAN/CSDL idealization is shown schematically in Figure 2 as it would appear in a stowed position. The element parameters are shown in Tables 7, 8 and 9 as taken from [6]. The payload mass of 32K lbs. is assumed distributed in a right circular cylinder 180 in. in diameter and 720 in. in length. The orbiter was assumed fixed in these analyses so its inertia is irrelevant.

ASAD/CSDL Model Details. The ASAD/CSDL model is in this paper for comparisons of the finite element implementation of the consistent mass matrix. Unfortunately for present purposes there are other differences from the NASTRAN/CSDL model. The most significant differences are:

1. No elbow offset in ASAD
2. ASAD has circular cross sections in all beams
3. Shorter beam segments since joint compliances are represented by rotary springs with zero length.
4. Rigid joints about drive axis.

The ASAD/CSDL model is shown in Figure 3. Properties of the beam elements are shown in Table 10.

Arm Configuration Analyzed. Several standard configurations have been proposed for RMS analysis. The results shown are for the "S" configuration which places the arm in a straight line. This is a worst case resulting in the lowest natural frequencies.

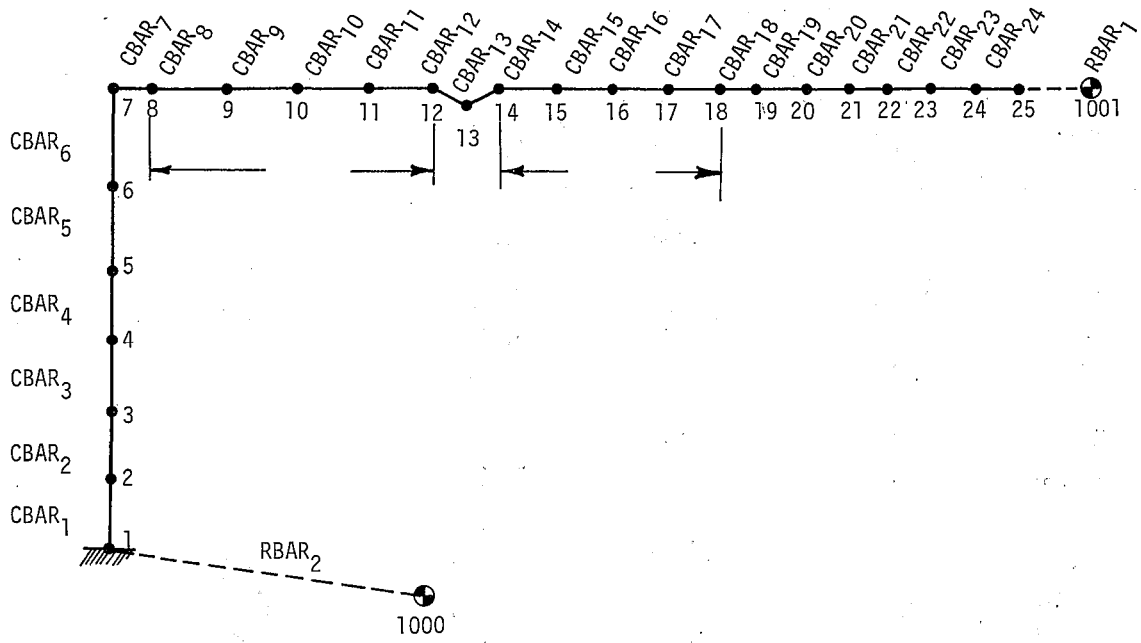


Fig. 2. CSDL Finite Element Idealization (NASTRAN) of Manipulator Arm in Stowed Configuration.

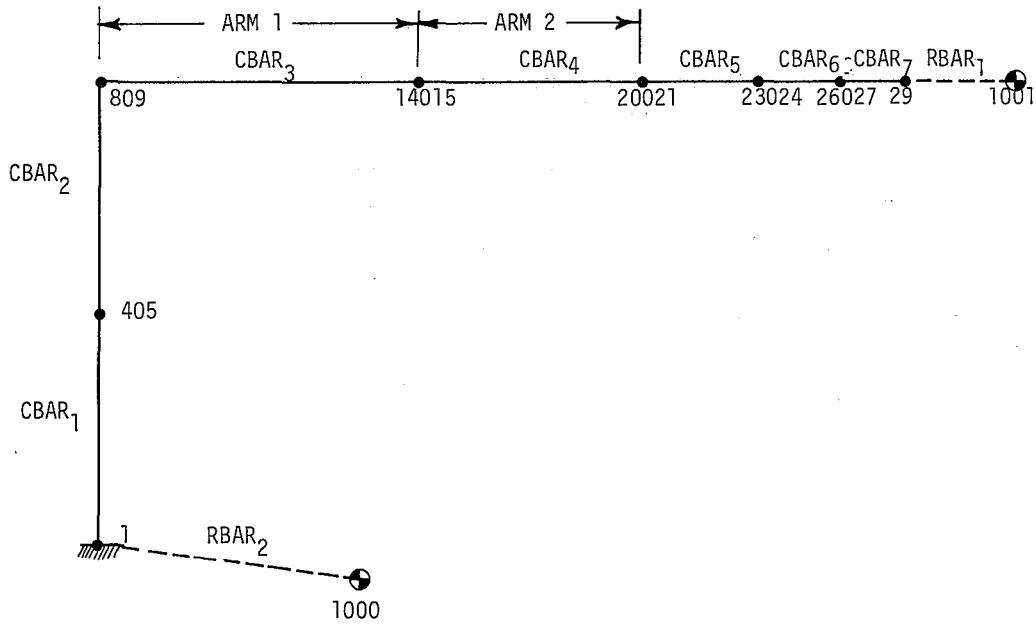


Fig. 3. ASAD/CSDL Finite Element Idealization of Manipulator Arm in Stowed Configuration (NASTRAN).

TABLE 7. Elastic Properties of Beam Elements,  
NASTRAN/CSDL Finite Element Model. [6]

CBAR <sub>i</sub>	Length (in.)	Cross-Sectional Area (in. <sup>2</sup> )	Polar Moment of Inertia (in. <sup>4</sup> )	Area Moment of Inertia, I <sub>1</sub> (in. <sup>4</sup> )	Area Moment of Inertia, I <sub>2</sub> (in. <sup>4</sup> )	Shear Factor
1	1.0	2.76	9.438	5.94	3.72	0.53 ↓ 0.53
2	1.25	2.76	9.438	5.94	3.72	
3	11.54	2.76	9.438	5.94	3.72	
4	11.0	13.7	228.8	35.7	35.7	
5	3.6	5.28	111.96	8.99	8.195	
6	8.4	2.276	61.524	51.41	19.74	
7	28.5	3.65	148.72	74.6	77.6	
8,9, 10,11	197.084	3.03	126.18	63.51	63.51	
12	25.5	3.98	138.84	40.9	101.0	
13	12.5	3.34	72.02	27.7	45.9	
14,15, 16,17	225.984	2.019	87.67	44.144	44.144	
18	39.5	1.450	84.24	38.4	47.8	
19	9.0	1.133	6.585	3.179	3.546	
20	9.0	1.133	7.943	4.23	3.877	
21	15.036	0.53	15.596	9.176	10.5	
22	14.919	1.266	12.81	6.567	6.567	
23	5.0	0.51	26.0	13.2	13.2	
24	18.0	2.55	77.48	7.2	7.21	

TABLE 8. Material Properties of Beam Elements,  
NASTRAN/CSDL Finite Element Model

CBAR <sub>i</sub>	E ≡ Young's Modulus (lbf/in <sup>2</sup> )	G ≡ Shear Modulus (lbf/in <sup>2</sup> )	ν ≡ Poissons Ratio
i=1,...,7,12 13,18,...,24	1.0*10 <sup>7</sup> (aluminum)	3.846*10 <sup>6</sup>	0.3
i=8,...,11, 14,...,17	2.22*10 <sup>7</sup> (graphite-epoxy)	5.635*10 <sup>6</sup>	0.97

TABLE 9. Concentrated Masses for NASTRAN/CSDL Finite Element Model.

Node	Mass (lb)	Mass(lbf-s <sup>2</sup> /in.)
3	12.63	0.0327
4	64.77	0.1676
5	61.74	0.1598
6	21.057	0.0545
7	49.133	0.1272
8	65.42	0.1693
9	23.3	0.0603
10	23.3	0.0603
11	23.3	0.0603
12	23.3	0.0603
13	146.47	0.3791
14	37.92	0.0981
15	16.81	0.0435
16	16.81	0.0435
17	16.81	0.0435
18	16.81	0.0435
19	82.40	0.2133
20	9.475	0.2452
21	9.475	0.2452
22	48.39	0.1252
23	48.01	0.1242
24	19.64	0.0508
25	70.70	0.1830
1001	32000.0	82.82

TABLE 10. Properties of Beam Elements - ASAD/CSDL Model.

Link	Length (in.)	Mass/Unit Length (lbf-s <sup>2</sup> /in. <sup>2</sup> )	Young's Modulus (lbf/in. <sup>2</sup> )	Shear Modulus (lbf/in. <sup>2</sup> )	Cross-Sectional Area (in. <sup>2</sup> )	Moment of Inertia I <sub>1</sub> = I <sub>2</sub> (in. <sup>4</sup> )	Polar Moment of Inertia (in. <sup>4</sup> )	Poissons Ratio $\nu$
1	22.536	0.01597	1.0*10 <sup>7</sup>	3.846*10 <sup>6</sup>	21.18	35.70	228.80	0.3
2	12.0	0.01517	1.0*10 <sup>7</sup>	3.846*10 <sup>6</sup>	24.22	46.70	158.30	0.3
3	251.076	0.003146	2.22*10 <sup>7</sup>	5.635*10 <sup>6</sup>	28.25	63.51	126.158	0.97
4	277.980	0.001746	2.22*10 <sup>7</sup>	5.635*10 <sup>6</sup>	23.55	44.144	87.652	0.97
5	18.0	0.002662	1.0*10 <sup>7</sup>	3.846*10 <sup>6</sup>	32.41	83.59	16.35	0.3
6	29.952	0.008330	1.0*10 <sup>7</sup>	3.846*10 <sup>6</sup>	14.31	16.301	31.720	0.3
7	23.00	0.01017	1.0*10 <sup>7</sup>	3.846*10 <sup>6</sup>	9.52	7.210	77.466	0.3